Chemical Science

ROYAL SOCIETY OF CHEMISTRY

EDGE ARTICLE

View Article Online
View Journal | View Issue

Cite this: *Chem. Sci.*, 2021, **12**, 9998

All publication charges for this article have been paid for by the Royal Society of Chemistry

Received 7th April 2021
Accepted 21st June 2021

DOI: 10.1039/d1sc01932e

rsc.li/chemical-science

A high-spin diradical dianion and its bridged chemically switchable single-molecule magnet†

Haiyan Cui, ‡[ab] Zhao-Bo Hu,‡[a] Chao Chen,‡[a] Huapeng Ruan,[a] Yong Fang,[a] Li Zhang,[d] Yue Zhao,[a] Gengwen Tan, *[c] You Song *[a] and Xinping Wang *[a]

Triplet diradicals have attracted tremendous attention due to their promising application in organic spintronics, organic magnets and spin filters. However, very few examples of triplet diradicals with singlet–triplet energy gaps (ΔE_{ST}) over 0.59 kcal mol^{-1} (298 K) have been reported to date. In this work, we first proved that the dianion of 2,7-di-*tert*-butyl-pyrene-4,5,9,10-tetraone (2,7-*t*Bu$_2$-PTO) was a triplet ground state diradical in the magnesium complex **1** with a singlet–triplet energy gap ΔE_{ST} = 0.94 kcal mol^{-1} (473 K). This is a rare example of stable diradicals with singlet–triplet energy gaps exceeding the thermal energy at room temperature (298 K). Moreover, the iron analog **2** containing the 2,7-*t*Bu$_2$-PTO diradical dianion was isolated, which was the first single-molecule magnet bridged by a diradical dianion. When **2** was doubly reduced to the dianion salt **2K$_2$**, single-molecule magnetism was switched off, highlighting the importance of diradicals in single-molecule magnetism.

Introduction

There is growing interest in radical chemistry because of the potential applications of radicals in various research fields such as organic chemistry, inorganic chemistry and materials science.[1] Diradicals are species containing two unpaired electrons that play pivotal roles in understanding the nature of chemical bonds and are of great interest in organic electronic device applications.[2] For example, Kubo and coworkers found that bisphenalenyl-based singlet diradicaloids exhibited high ambipolar mobilities in organic field-effect transistors[3] and strong two-photon absorption properties.[4] Attributed to the small HOMO–LUMO gaps, several singlet diradicaloids show strong absorption in the near-infrared (NIR) region and can be applied to NIR-organic photodetectors.[5] Triplet diradicals are particularly attractive regarding their promising usage in organic magnets, organic spintronics,[6] spin filters,[7] memory devices,[8] *etc.* The well-known triplet diradical *m*-xylylene possesses a large singlet–triplet energy gap (ΔE_{ST}) of *ca.* 9.6 kcal mol^{-1},[9] but it is only observable in solution at room temperature for hundreds of nanoseconds.[10] Rajca group reported a triplet aza-*m*-xylylene diradical with ΔE_{ST} around 10 kcal mol^{-1}, which was persistent at ambient temperature in solution on the time scale of minutes.[11] To date, the number of stable triplet diradicals with ΔE_{ST} over 0.59 kcal mol^{-1} (298 K), *i.e.*, surpassing the thermal energy at room temperature, remains limited due to the intrinsic high reactivity.[2f,12]

In contrast, the application of diradicals in synthesizing single-molecule magnets (SMMs) is much less explored, although monoradicals have been widely utilized in designing SMMs.[13] In the studied diradical-containing SMMs, the diradicals are mainly composed of neutral bis(imino nitroxide) moieties.[14] However, neutral diradicals often suffer from weak coordination to metal ions. In recent years, a few stable triplet ground state diradicals with ΔE_{ST} over 298 K have been realized by electron delocalization and steric protection strategies.[15] Thus, it is highly desirable to apply these high-spin diradicals to design SMMs. Shultz and coworkers obtained a series of bis(-semiquinone) diradical dianion metal complexes with large ΔE_{ST} over 298 K, but none of them are SMMs.[16]

In this contribution, we report a readily accessible 2,7-di-*tert*-butyl-pyrene-4,5,9,10-tetraone (2,7-*t*Bu$_2$-PTO) diradical dianion in the magnesium and iron complexes LMg^{II}(2,7-*t*Bu$_2$-PTO)Mg^{II}L (L = CH(MeCNAr)$_2$, Ar = 2,6-iPr$_2$C$_6$H$_3$) **1** and LFe^{II}(2,7-*t*Bu$_2$-PTO)Fe^{II}L **2**, respectively. Complex **1** features a triplet ground state with ΔE_{ST} = 0.94 kcal mol^{-1} (473 K). Complex **2** represents the first SMM connected by a strong ferromagnetically coupled diradical dianion. Moreover, **1** and **2** can be

[a]*State Key Laboratory of Coordination Chemistry, Jiangsu Key Laboratory of Advanced Organic Materials, School of Chemistry and Chemical Engineering, Collaborative Innovation Center of Advanced Microstructures, Nanjing University, Nanjing 210023, China. E-mail: xpwang@nju.edu.cn; yousong@nju.edu.cn*

[b]*Jiangsu Key Laboratory of Pesticide Science, College of Sciences, Nanjing Agricultural University, Nanjing 210095, China*

[c]*College of Chemistry, Chemical Engineering and Materials Science, Soochow University, Suzhou 215123, China. E-mail: gwtan@suda.edu.cn*

[d]*Center of Materials Science and Engineering, Guangxi University of Science and Technology, Liuzhou 545006, China*

† Electronic supplementary information (ESI) available: Experimental details, all characterization data and theoretical calculation details. CCDC 1998479–1998482. For ESI and crystallographic data in CIF or other electronic format see DOI: 10.1039/d1sc01932e

‡ These authors contributed equally to this work.

further doubly reduced to dianion salts $\mathbf{1K_2}$ and $\mathbf{2K_2}$, where the 2,7-tBu$_2$-PTO units are in the diamagnetic tetraanion state, and the single-molecule magnetism of $\mathbf{2K_2}$ is switched off.

Results and discussion

Syntheses and two-electron reduction of the 2,7-tBu$_2$-PTO diradical dianion ligated magnesium and iron complexes

Pyrene-4,5,9,10-tetraones have been widely used as electronic materials due to their intrinsic strong π-electron acceptor ability.[17] They can accept as many as four electrons. However, the molecular and electronic structures of the reduced species, especially the doubly reduced species, have never been fully elucidated.[18] The cyclic voltammograms reveal that 2,7-tBu$_2$-PTO can undergo four reversible one-electron reduction events with reduction potentials at −0.431 V, −0.710 V, −0.884 V and −1.556 V *versus* the Ag/Ag$^+$ electrode (Fig. S1†), which indicates that the reduced species may be isolable.

The β-diketiminato-ligated magnesium dimer reported by Jones and coworkers,[19] which has been proven to be an elegant reducing agent in synthetic chemistry,[20] was utilized to reduce 2,7-tBu$_2$-PTO. The reaction of 2,7-tBu$_2$-PTO and one molar equivalent of LMg^{I}–Mg^{I}L in toluene at room temperature resulted in deep green crystals of **1** after workup (Fig. 1). It has been spectroscopically and structurally characterized. Intrigued by the facile access of **1** and our previous phosphorus radical anion-coordinated Fe^{II} complex exhibiting single-molecule magnetic properties,[21] we were interested in applying the 2,7-tBu$_2$-PTO diradical dianion to construct SMMs. Then, the reaction of 2,7-tBu$_2$-PTO and two molar equivalents of LFe^{I}(toluene)[22] was performed in toluene at room temperature, from which reddish brown crystals of **2** were isolated (Fig. 1). Complexes **1** and **2** are highly sensitive to oxygen and moisture but can be stored for months in an N_2-filled glovebox at ambient temperature.

The cyclic voltammetric investigations (Fig. S2 and S3†) show that compounds **1** and **2** exhibit two reversible reduction waves ($E^{red}_{1/2}$ = −1.811 V and −1.548 V for **1**; $E^{red}_{1/2}$ = −0.194 V and −0.974 V for **2** *vs.* Ag/Ag$^+$), indicating that **1** and **2** can be doubly reduced. In addition, a reversible oxidation process was observed at $E_{1/2}$ = 0.077 V for **2**, suggesting that it can also be oxidized, which might be attributed to the oxidation of the reduced form of 2,7-tBu$_2$-PTO. Consequently, reactions of **1** and **2** with two molar equivalents of elemental potassium in THF at room temperature led to the formation of dianion salts $\mathbf{1K_2}$ and $\mathbf{2K_2}$, respectively, which were isolated in moderate yields (Fig. 2). The solution NMR spectroscopic studies of $\mathbf{1K_2}$ at room temperature show well-resolved ^{1}H and ^{13}C signals in the diamagnetic window (Fig. S11 and S12,† respectively). The ^{1}H NMR spectrum exhibits a singlet resonance at δ 8.42 ppm for the hydrogen atoms of the pyrene moiety. The proton signal for the γ-H of the β-diketiminato ligand (δ = 5.10 ppm) in $\mathbf{1K_2}$ is slightly downfield shifted compared to that of the β-diketiminato ligated magnesium dimer (δ = 4.81 ppm).

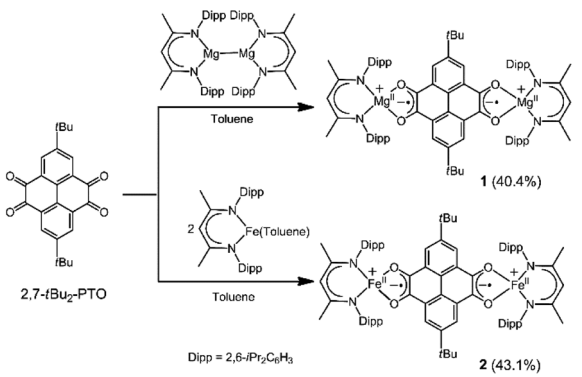

Fig. 1 Syntheses of complexes **1** and **2**.

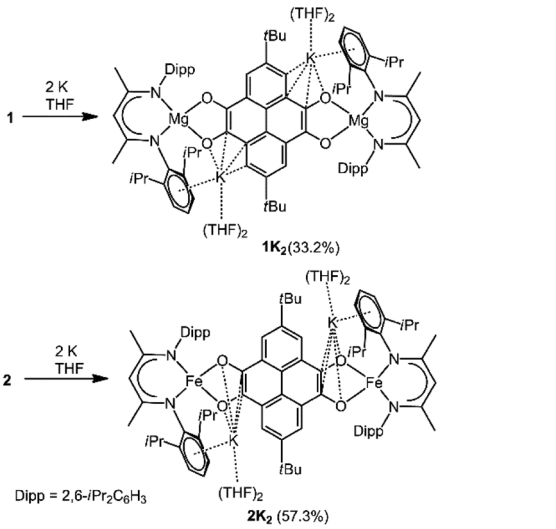

Fig. 2 Two-electron reduction of **1** and **2** affording $\mathbf{1K_2}$ and $\mathbf{2K_2}$, respectively.

Crystal structures

Crystals of **1** were obtained by cooling the toluene solution at −20 °C (Fig. 3A).[23] It crystallizes in the monoclinic space group $P2_1/c$ and features a centrosymmetric geometry. The Mg atoms feature a tetrahedral geometry. The Mg–O distances (1.9803(19) and 1.9714(19) Å) are comparable to those of the magnesium oxalate compound LMg(μ-C_2O_4)MgL (1.9855(15) and 1.9858(14) Å).[24] The C–O bonds are elongated, while the C7–C8 bond is shortened in comparison to those in 2,7-tBu$_2$-PTO (Table 1)[25] in accordance with the reduction of carbonyl compounds. The C7–C8 bond length (1.443(3) Å) is between those of the C–C single bond (1.54 Å) and C=C double bond (1.34 Å), which shows the semiquinone character of the C_2O_2 moieties. Moreover, due to the steric bulkiness of the L ligands, no intermolecular interaction is observed, which is normally present in pyrenes.[26]

The molecular configuration of **2** is akin to that of **1** (Fig. 3B). The iron centers feature a tetrahedral geometry. The Fe–N bond lengths (1.963(2) and 1.968(2) Å) are comparable to those in the diazafluorenylidene-substituted phosphaalkene radical anion coordinated iron complex (1.980(2) and 1.968(2) Å).[21] The bond lengths in the 2,7-tBu$_2$-PTO moiety of **2** are comparable to those

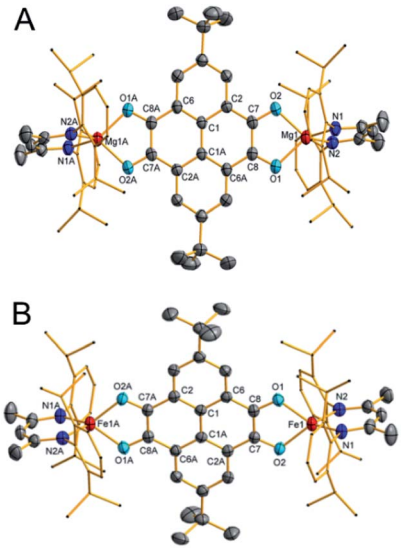

Fig. 3 Thermal ellipsoid drawing of the molecular structures of **1** (A) and **2** (B) at 50% probability. Hydrogen atoms are omitted for clarity. Selected bond lengths (Å) and angles (°): **1**: Mg1–O1 1.9803(19), Mg1–O2 1.9714(19), Mg1–N1 2.007(2), Mg1–N2 2.011(2), O1–C8 1.292(3), O2–C7 1.289(3), C1A–C6A 1.414(3), C1A–C2 1.405(3), C2–C7 1.441(3), C6A–C8 1.438(3), C7–C8 1.443(3), O2–Mg1–O1 83.88(7), O2–Mg1–N1 117.37(9), O1–Mg1–N1 127.47(9), O2–Mg1–N2 118.65(9), O1–Mg1–N2 116.80(9), and N1–Mg1–N2 95.13(9). **2**: Fe1–N1 1.963(2), Fe1–N2 1.968(2), Fe1–O2 1.992(2), Fe1–O1 2.0014(19), O1–C8 1.291(3), O2–C7 1.295(3), C1A–C2A 1.408(4), C1–C1A 1.449(5), C1–C6 1.400(4), C2A–C7 1.445(4), C7–C8 1.422(4), C6–C8 1.443(4), N1–Fe1–N2 95.08(10), N1–Fe1–O2 128.34(9), N2–Fe1–O2 118.58(9), N1–Fe1–O1 117.52(9), N2–Fe1–O1 118.75(9), and O2–Fe1–O1 80.97(8). Symmetry transformations were used to generate equivalent atoms labeled with 'A': $-x + 1$, $y + 1$, and $z + 1$.

in **1** (Table 1), which suggest that 2,7-*t*Bu$_2$-PTO is also most likely in the diradical dianion state. Therefore, two-electron transfer to 2,7-*t*Bu$_2$-PTO occurs in the reaction, and the iron atoms are in the oxidation state of two. Additionally, the zero-field ^{57}Fe Mössbauer spectrum recorded at 80 K afforded an isomer shift value $\delta = 0.86$ mm s^{-1} and a quadrupole splitting value $\Delta E_Q = 1.87$ mm s^{-1} (Fig. S4†), which confirms the presence of high-spin tetrahedral Fe^{II} ions in **2**.[21,27]

Crystals of **1K$_2$** and **2K$_2$** suitable for X-ray diffraction analysis were grown from THF solutions at −20 °C (Fig. 4). They crystallize in the monoclinic space group $P\bar{1}$. In comparison to precursors **1** and **2**, the M–N bonds (2.044(2) and 2.045(2) Å for **1K$_2$**; 1.997(2) and 1.9938(19) Å for **2K$_2$**) are slightly elongated, while the M–O bonds (1.9300(18) and 1.9506(18) Å for **1K$_2$**; 1.9808(15) and 1.9811(16) Å for **2K$_2$**) are shortened. The most pronounced change is the further increased C–O bond lengths (Table 1), which are close to those in the pyrocatecholate aluminum compound (1.369(5) and 1.380(4) Å).[28] Meanwhile, C7–C8 bonds (1.382(3) Å for **1K$_2$**; 1.390(3) Å for **2K$_2$**) are shortened, compared with those of **1** and **2**. So 2,7-*t*Bu$_2$-PTO is in the tetraanion form. This result is consistent with the diamagnetic nature of **1K$_2$** demonstrated by NMR spectroscopy. Moreover, the isomer shift value $\delta = 0.86$ mm s^{-1} and quadrupole splitting value $\Delta E_Q = 1.57$ mm s^{-1} obtained from the zero-field ^{57}Fe Mössbauer spectrum at 80 K of **2K$_2$** (Fig. S5†) are close to those of **2**, which prove the retention of the high-spin +2 oxidation state of the iron centers.

Table 1 Selected bond lengths (Å) of 2,7-^{t}Bu$_2$-PTO, **1**, **2**, **1K$_2$** and **2K$_2$**

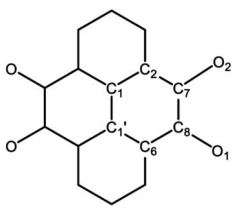

	2,7-*t*Bu$_2$-PTO[25]	**1**	**2**	**1K$_2$**	**2K$_2$**
C7–O2	1.221(7)	1.289(3)	1.295(3)	1.362(3)	1.344(3)
C8–O1	1.209(7)	1.292(3)	1.291(3)	1.343(3)	1.347(2)
C7–C8	1.545(8)	1.443(3)	1.422(4)	1.382(3)	1.390(3)
C6–C8	1.497(8)	1.438(3)	1.443(4)	1.441(3)	1.429(3)
C1′–C6	1.416(8)	1.414(3)	1.400(4)	1.419(3)	1.423(3)
C1–C1′	1.474(11)	1.437(4)	1.449(5)	1.411(4)	1.415(4)
C1–C2	1.401(7)	1.405(3)	1.408(4)	1.425(3)	1.420(3)
C2–C7	1.472(8)	1.441(3)	1.445(4)	1.434(3)	1.435(3)

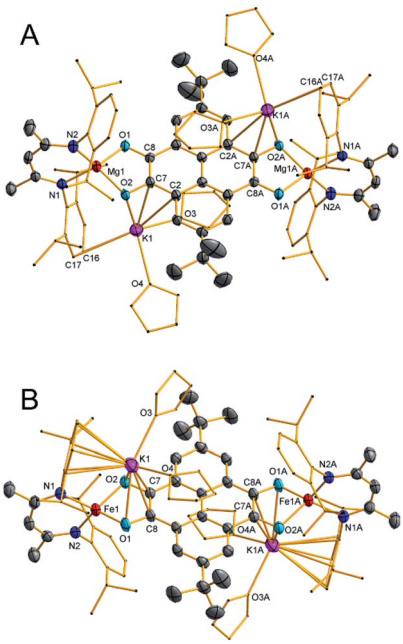

Fig. 4 Thermal ellipsoid drawing of the molecular structures of **1K$_2$** (A) and **2K$_2$** (B) at 50% probability. Hydrogen atoms are omitted for clarity. Symmetry transformations were used to generate equivalent atoms labeled with 'A': $-x + 1$, $y + 1$, and $z + 1$. Selected bond lengths (Å) and angles (°): **1**: Mg1–O1 1.9300(18), Mg1–O2 1.9506(18), Mg1–N1 2.044(2), Mg1–N2 2.045(2), O1–C8 1.343(3), O2–C7 1.362(3), C7–C8 1.382(3), O1–Mg1–O2 88.12(7), O1–Mg1–N1 124.02(8), O2–Mg1–N1 111.77(8), O1–Mg1–N2 119.64(9), O2–Mg1–N2 123.41(8), and N1–Mg1–N2 92.79(8). **2**: Fe1–O2 1.9808(15), Fe1–O1 1.9811(16), Fe1–N2 1.997(2), Fe1–N1 1.9938(19), O1–C8 1.347(2), O2–C7 1.344(3), C7–C8 1.390(3), O2–Fe1–O1 83.55(6), O2–Fe1–N2 122.09(7), O1–Fe1–N2 124.11(8), O2–Fe1–N1 115.24(7), O1–Fe1–N1 120.34(7), and N2–Fe1–N1 94.10(8).

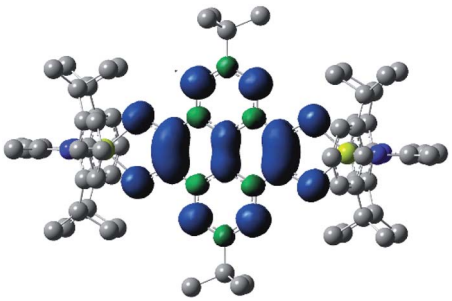

Fig. 5 Spin density distribution of **1** in the triplet state calculated at the UB3LYP/6-31G(d) level (isovalue = 0.002 a.u.).

Calculated electron spin density distribution and singlet–triplet gap of 1

The theoretical calculations of **1** were performed. Geometry optimizations were performed at the (U)B3LYP/6-31G(d) level, and the stationary points were checked by frequency calculations.[29] The results from theoretical calculations are interpreted to suggest that **1** has a triplet ground state, and the calculated singlet–triplet gap is 0.91 kcal mol^{-1}. Moreover, the spin density distribution shows that it is mainly delocalized over the two C_2O_2 moieties with contributions from the two central benzene rings (Fig. 5).

Magnetic characterization

Electro-paramagnetic resonance (EPR) spectroscopy and superconducting quantum interference device (SQUID) measurements were performed to clarify the electronic structures of newly formed complexes. The EPR spectrum of **1** in the frozen toluene solution at 90 K (Fig. 6A) reveals a clear half-field signal of the forbidden transition ($\Delta m_s = \pm 2$), which indicates the presence of a triplet-spin state species. The signals attributed to the $\Delta m_s = \pm 1$ transition are finely resolved, and parameters $g_x = g_y = 2.0028$, $g_z = 2.0042$, $D = 139$ G and $E = 32$ G are extracted from the spectral simulation with the SimFonia software package. From the zero-field splitting parameter D, the distance between the spin centers is estimated to be 5.85 Å,[2f] which is close to the mean distance (6.05 Å) of C7 to C8A and O2 to O1A in the solid-state structure, which suggests that the spin density is delocalized over the C_2O_2 moieties. In contrast, iron complexes **2** and **2K$_2$** are EPR-silent at room temperature and 90 K.

SQUID measurements were performed on the powder sample of **1** (Fig. 6B). The $\chi_M T$ value at 300 K is 0.83 cm^3 mol^{-1} K, which is larger than the theoretical value of 0.75 cm^3 mol^{-1} K ($S = 1/2$, $g = 2.0$) for 2 free radicals. With decreasing temperature, the $\chi_M T$ values slowly increase to a maximum of 1.04 cm^3 mol^{-1} K at 8 K. With the further decrease in temperature, the $\chi_M T$ values slightly decline to 1.0 cm^3 mol^{-1} K at 1.8 K. This behavior obviously indicates a strong ferromagnetic coupling between two $S = 1/2$ centers in **1**, and the spins are completely parallel below 8 K. Moreover, the isothermal magnetization of 1.96 Nμ_B at 70 kOe and 1.8 K is close to the theoretical value of 2 Nμ_B ($S = 1$, $g = 2$) (Fig. S6†), which provides evidence of ferromagnetic coupling. The temperature-dependent magnetizations were fitted using the PHI program based on equation $\hat{H} = -2J\hat{S}_1\hat{S}_2 + g\mu_B\hat{S}H$ ($S_1 = S_2 = 1/2$). The best fitting results are $g = 2.04(1)$, $J = 165.1(5)$ cm^{-1}, $zj = -0.0053(1)$ cm^{-1} and TIP = 4.17 $\times$ 10^{-4} cm^3 mol^{-1}. Hence, complex **1** is a triplet ground state diradical with a singlet–triplet energy gap of 0.94 kcal mol^{-1} (473 K), and there is negligible intermolecular interaction. The experimental results are consistent with the theoretical calculations. Complex **1** is a rare example of stable diradicals with singlet–triplet energy gaps larger than 0.6 kcal mol^{-1} (300 K).

SQUID measurements on the powder samples of **2** and **2K$_2$** were also performed to gain more insights into their electronic structures and magnetic properties. The $\chi_M T$ value of 5.26 cm^3 mol^{-1} K at 300 K for **2** (Fig. 7) is far less than 6.75 cm^3 mol^{-1} K for two high-spin Fe^{II} ions ($S = 2$, $g = 2.0$) and two organic radicals ($S = 1$, $g = 2.0$). This phenomenon may be due to

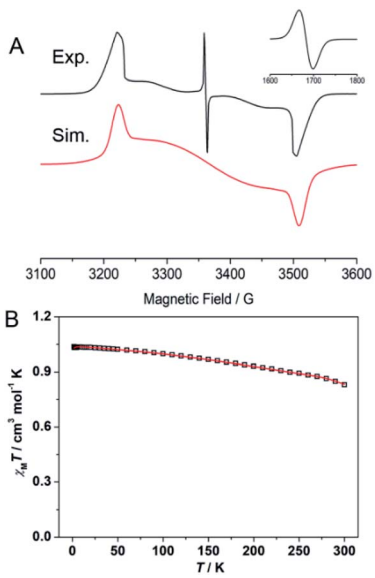

Fig. 6 (A) Experimental (black line) and simulated (red line) EPR spectra of **1** in toluene solution at 90 K. The central peak is attributed to the $S = 1/2$ monoradical impurity. (B) $\chi_M T$–T plots of **1** with the fitting results (red line).

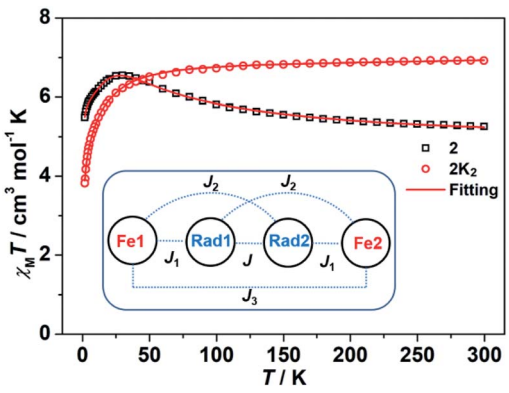

Fig. 7 $\chi_M T$–T plots of **2** and **2K$_2$** with the fitting results (red line) using the PHI program. The inset shows the magnetic coupling situation in **2**.

a strong antiferromagnetic coupling between the metal ions and the diradical ions, which results in dominant magnetic properties even above room temperature. With decreasing temperature, the $\chi_M T$ values first gradually increase from 300 to 30 K, subsequently show a pronounced decrease, and finally reach the ultimate value of 5.48 $cm^3\ mol^{-1}$ K at 1.8 K. This phenomenon should be attributed to the competition between the intramolecular ferromagnetic and antiferromagnetic coupling, which forms a ferromagnetic experimental curve. The temperature and field dependent magnetizations were fitted to quantify the anisotropy parameters based on eqn (1) using the PHI program:

$$\hat{H} = -2J_1\left(\hat{S}_{Fe1}\hat{S}_{Rad1} + \hat{S}_{Rad2}\hat{S}_{Fe2}\right) - 2J\hat{S}_{Rad1}\hat{S}_{Rad2} - 2J_2\left(\hat{S}_{Fe1}\hat{S}_{Rad2} + \hat{S}_{Rad1}\hat{S}_{Fe2}\right) - 2J_3\hat{S}_{Fe1}\hat{S}_{Fe2} + D\left[\hat{S}_z{}^2 - \frac{S(S+1)}{3}\right] + g\mu_B\hat{S}H \quad (1)$$

where J and J_1–J_3 are the magnetic coupling constants between the spins of radicals and Fe^{II} ions (Fig. 7, inset). A reasonable fitting gives $D = -10.0(2)\ cm^{-1}$, $g = 2.23(1)$, $J_1 = -634.7(4)$, $J = 116.1(1)$, $J_2 = -7.37(10)$, $J_3 = -0.11(1)\ cm^{-1}$ and TIP $= 5.93 \times 10^{-4}\ cm^3\ mol^{-1}$. The results indicate that the high-spin Fe^{II} ions exhibit very strong antiferromagnetic coupling with the diradical unit. The coupling constant magnitude ($-634.7(4)\ cm^{-1}$) is similar to that observed in the azophenine radical-bridged dinuclear iron complex ($|J| \geq 900\ cm^{-1}$).[30] Moreover, the ferromagnetic coupling of the diradical dianion is retained in **2**, and the coupling constant is slightly lower than that in **1** because the electronic structure has changed, such as the angle O1–Mg1–O2 from 83.87° for **1** to 80.97° for **2**. The magnetization of 4.16 $N\mu_B$ at 7 T and 1.8 K is far less than the expected value of 6.0 $N\mu_B$ due to the strong anisotropy, which is also shown by the non-superposition of the *M vs. H*/*T* plots (Fig. S8†).

The $\chi_M T$ value of $\mathbf{2K_2}$ at 300 K is 6.92 $cm^3\ mol^{-1}$ K, and the value first slowly decreases from room temperature to 60 K and subsequently rapidly decreases to 3.82 $cm^3\ mol^{-1}$ K at 1.8 K (Fig. 7). These results suggest that the two high-spin Fe^{II} ions are weakly antiferromagnetically coupled in $\mathbf{2K_2}$. Fitting the $\chi_M T$–T plots to eqn (2) using the PHI program[31] yields the parameters of $D = -6.45(10)\ cm^{-1}$, $g = 2.12(2)$, $J_3 = -0.028(1)\ cm^{-1}$ and TIP $= 7.22 \times 10^{-4}\ cm^3\ mol^{-1}$. The weak coupling between the Fe^{II} ions is due to the closed-shell character of the 2,7-*t*Bu_2-PTO tetraanion, as observed in $\mathbf{1K_2}$. The large difference in the D value in complexes **2** and $\mathbf{2K_2}$ can be attributed to the change in the local ligand field after the two-electron reduction.

$$\hat{H} = -2J_3\hat{S}_{Fe1}\hat{S}_{Fe2} + D\left[\hat{S}_z{}^2 - \frac{S(S+1)}{3}\right] + g\mu_B\hat{S}H \quad (2)$$

Alternating current (ac) susceptibility measurements were performed to evaluate the magnetization dynamics of **2** and $\mathbf{2K_2}$. Obvious out-of-phase signals (χ_M'') were observed for **2** under a zero field, whereas no peak was observed below 1000 Hz (Fig. S9†), which suggests the existence of quantum tunneling of magnetization (QTM). In contrast, the susceptibility measurements of $\mathbf{2K_2}$ showed that no χ_M'' signals were observed with or without external fields, which suggests switching off the single-molecule magnetism after the two-electron reduction of **2**.

To suppress the QTM effect, a 1.0 kOe field was applied to study the slow relaxation behavior of **2**. The frequency-dependent in-of-phase signals (χ_M', Fig. S10†) and χ_M'' (Fig. 8A) are observed in the temperature range of 1.8–5 K. The Cole–Cole plots of χ_M'' *versus* χ_M' were fitted using the CC-FIT program and a modified Debye function (Fig. 8B). The extracted α values are listed in Table S2 in the ESI† and are less than 0.1, which indicates a narrow distribution of relaxation times. The relaxation time τ_0 and effective barrier energy were afforded by fitting the Arrhenius-like diagrams (Fig. 8C). The entire temperature dataset was fitted using the equation $\tau^{-1} = AT + CT^{-n} + \tau_0{}^{-1}\exp(-U_{eff}/k_BT)$, where A is the coefficient of the direct process, C is the coefficient of the Raman process, U_{eff} is the energy barrier for magnetization reversal, and k_B is the Boltzmann constant. The best fitting parameters are $A = 29.68\ K^{-1}\ s^{-1}$, $C = 4.66\ K^{-3.03}\ s^{-1}$, $n = 3.03$, $\tau_0 = 7.33 \times 10^{-11}$ s and

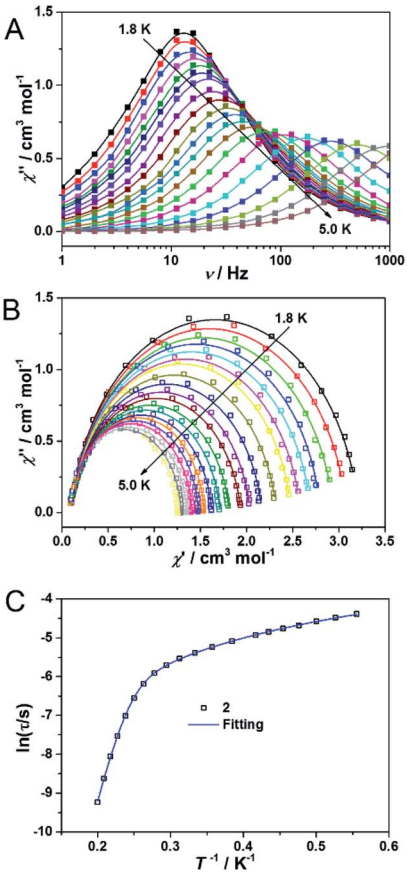

Fig. 8 (A) Frequency dependence of the out-of-phase (χ_M'') ac-susceptibilities for **2** at different temperatures under a 1.0 kOe field. (B) Cole–Cole curves under a 1.0 kOe field for **2**. (C) Plots of ln(τ/s) *versus* T^{-1} under a 1.0 kOe field for **2**.

$U_{eff} = 71.1$ K. The fitting results indicate that the QTM effect has been suppressed well by the applied magnetic field.

Conclusions

We have first demonstrated that the dianion of 2,7-tBu$_2$-PTO is a triplet ground state diradical in the coordination sphere of magnesium. This is a rare example of stable diradicals with singlet–triplet energy gaps larger than 0.59 kcal mol^{-1} (298 K), which surpasses the thermal energy at room temperature. The diradical dianion was applied to synthesize iron complex **2**, which serves as the first SMM bridged by a diradical dianion. Complexes **1** and **2** can be reduced to dianion salts $\mathbf{1K_2}$ and $\mathbf{2K_2}$, respectively, where the 2,7-tBu$_2$-PTO units are in diamagnetic tetraanion form. This work provides more insights into the molecular and electronic structures of the reduced species of PTO and demonstrates the potential of diradical dianions in constructing interesting magnetic materials. Syntheses and magnetic studies of other complexes bearing the reduced species of PTO are ongoing in our laboratory.

Data availability

Crystallographic data for **1**, **2**, $\mathbf{1K_2}$ and $\mathbf{2K_2}$ have been deposited in the Cambridge Crystallographic Data Center under CCDC No. 1998479–1998482.

Author contributions

X. W. conceived the project. H. C. conducted the synthesis and physical characterizations. Z. H. and Y. S. performed the magnetic analysis. C. C. performed the SQUID measurements. H. R. and Y. Z. performed the crystallographic measurements and data refinements. Y. F. performed the EPR measurements. L. Z. performed the DFT calculations. G. T. wrote the manuscript. H. C. wrote the experimental part. G. T., Y. S. and X. W. revised the manuscript.

Conflicts of interest

There are no conflicts to declare.

Acknowledgements

We thank the National Key R&D Program of China (2016YFA0300404, 2017YFA0303203 and 2018YFA0306004), National Natural Science Foundation of China (21402094, 21525102, 21690062 and 21973038), China Postdoctoral Science Foundation (2017M611774) and the Joint Fund for Regional Innovation and Development (U20A2073) for financial support. L. Z. thanks the Guangxi Department of Science and Technology (AD19245107) and Guangxi University of Science and Technology (03190227 and 03190228) for financial support. The calculations were performed at the High-Performance Computing Center of Nanjing University. We thank Ms Jie Xiao and Prof. Liang Deng of Shanghai Institute of Organic Chemistry for measuring the Mössbauer spectra.

Notes and references

1 (*a*) P. P. Power, *Chem. Rev.*, 2003, **103**, 789–809; (*b*) R. G. Hicks, in *Stable Radicals: Fundamentals and Applied Aspects of Odd-Electron Compounds*, John Wiley & Sons, Ltd, 2010; (*c*) M. Mas-Torrent, N. Crivillers, C. Rovira and J. Veciana, *Chem. Rev.*, 2012, **112**, 2506–2527; (*d*) I. Ratera and J. Veciana, *Chem. Soc. Rev.*, 2012, **41**, 303–349; (*e*) T. Chivers and J. Konu, in *Comprehensive Inorganic Chemistry II*, ed. K. Poeppelmeier, Elsevier, Amsterdam, 2nd edn, 2013, pp. 349–373; (*f*) G. Tan and X. Wang, *Chin. J. Chem.*, 2018, **36**, 573–586.

2 (*a*) L. Salem and C. Rowland, *Angew. Chem., Int. Ed.*, 1972, **11**, 92–111; (*b*) W. T. Borden, *Diradicals*, Wiley-Interscience, New York, 1982; (*c*) A. Rajca, *Chem. Rev.*, 1994, **94**, 871–893; (*d*) F. Breher, *Coord. Chem. Rev.*, 2007, **251**, 1007–1043; (*e*) Z. Sun, Q. Ye, C. Chi and J. Wu, *Chem. Soc. Rev.*, 2012, **41**, 7857–7889; (*f*) M. Abe, *Chem. Rev.*, 2013, **113**, 7011–7088; (*g*) N. M. Gallagher, A. Olankitwanit and A. Rajca, *J. Org. Chem.*, 2015, **80**, 1291–1298; (*h*) Z. Zeng, X. Shi, C. Chi, J. T. Lopez Navarrete, J. Casado and J. Wu, *Chem. Soc. Rev.*, 2015, **44**, 6578–6596; (*i*) G. Tan and X. Wang, *Acc. Chem. Res.*, 2017, **50**, 1997–2006.

3 (*a*) T. Kubo, A. Shimizu, M. Sakamoto, M. Uruichi, K. Yakushi, M. Nakano, D. Shiomi, K. Sato, T. Takui, Y. Morita and K. Nakasuji, *Angew. Chem., Int. Ed.*, 2005, **44**, 6564–6568; (*b*) H. Koike, M. Chikamatsu, R. Azumi, J. y. Tsutsumi, K. Ogawa, W. Yamane, T. Nishiuchi, T. Kubo, T. Hasegawa and K. Kanai, *Adv. Funct. Mater.*, 2016, **26**, 277–283.

4 K. Kamada, K. Ohta, T. Kubo, A. Shimizu, Y. Morita, K. Nakasuji, R. Kishi, S. Ohta, S.-i. Furukawa, H. Takahashi and M. Nakano, *Angew. Chem., Int. Ed.*, 2007, **46**, 3544–3546.

5 (*a*) A. Konishi, Y. Hirao, M. Nakano, A. Shimizu, E. Botek, B. Champagne, D. Shiomi, K. Sato, T. Takui, K. Matsumoto, H. Kurata and T. Kubo, *J. Am. Chem. Soc.*, 2010, **132**, 11021–11023; (*b*) Z. Zeng, S. Lee, J. L. Zafra, M. Ishida, X. Zhu, Z. Sun, Y. Ni, R. D. Webster, R.-W. Li, J. T. López Navarrete, C. Chi, J. Ding, J. Casado, D. Kim and J. Wu, *Angew. Chem., Int. Ed.*, 2013, **52**, 8561–8565; (*c*) Y. Zheng, M.-s. Miao, G. Dantelle, N. D. Eisenmenger, G. Wu, I. Yavuz, M. L. Chabinyc, K. N. Houk and F. Wudl, *Adv. Mater.*, 2015, **27**, 1718–1723; (*d*) Y. Ni, S. Lee, M. Son, N. Aratani, M. Ishida, A. Samanta, H. Yamada, Y.-T. Chang, H. Furuta, D. Kim and J. Wu, *Angew. Chem., Int. Ed.*, 2016, **55**, 2815–2819.

6 (*a*) A. R. Rocha, V. M. Garcia-suarez, S. W. Bailey, C. J. Lambert, J. Ferrer and S. Sanvito, *Nat. Mater.*, 2005, **4**, 335–339; (*b*) S. Sanvito, *Chem. Soc. Rev.*, 2011, **40**, 3336–3355.

7 (*a*) C. Herrmann, G. C. Solomon and M. A. Ratner, *J. Am. Chem. Soc.*, 2010, **132**, 3682–3684; (*b*) S. Shil, D. Bhattacharya, A. Misra and D. J. Klein, *Phys. Chem. Chem. Phys.*, 2015, **17**, 23378–23383.

8 (*a*) Y. Yonekuta, K. Susuki, K. Oyaizu and K. Honda, *J. Am. Chem. Soc.*, 2007, **129**, 14128–14129; (*b*) J. Lehmann, A. Gaita-Ariño, E. Coronado and D. Loss, *J. Mater. Chem.*,

2009, **19**, 1672–1677; (*c*) K. Oyaizu and H. Nishide, *Adv. Mater.*, 2009, **21**, 2339–2344; (*d*) R. Gaudenzi, J. de Bruijckere, D. Reta, I. d. P. R. Moreira, C. Rovira, J. Veciana, H. S. J. van der Zant and E. Burzurí, *ACS Nano*, 2017, **11**, 5879–5883.

9 (*a*) B. B. Wright and M. S. Platz, *J. Am. Chem. Soc.*, 1983, **105**, 628–630; (*b*) P. G. Wenthold, J. B. Kim and W. C. Lineberger, *J. Am. Chem. Soc.*, 1997, **119**, 1354–1359; (*c*) P. Neuhaus, D. Grote and W. Sander, *J. Am. Chem. Soc.*, 2008, **130**, 2993–3000.

10 K. W. Haider, E. Migirdicyan, M. S. Platz, N. Soundararajan and A. Despres, *J. Am. Chem. Soc.*, 1990, **112**, 733–738.

11 A. Rajca, A. Olankitwanit and S. Rajca, *J. Am. Chem. Soc.*, 2011, **133**, 4750–4753.

12 T. Stuyver, B. Chen, T. Zeng, P. Geerlings, F. De Proft and R. Hoffmann, *Chem. Rev.*, 2019, **119**, 11291–11351.

13 (*a*) S. Demir, I.-R. Jeon, J. R. Long and T. D. Harris, *Coord. Chem. Rev.*, 2015, **289–290**, 149–176; (*b*) L. Wang, J. Li, L. Zhang, Y. Fang, C. Chen, Y. Zhao, Y. Song, L. Deng, G. Tan, X. Wang and P. P. Power, *J. Am. Chem. Soc.*, 2017, **139**, 17723–17726; (*c*) X. Meng, W. Shi and P. Cheng, *Coord. Chem. Rev.*, 2019, **378**, 134–150.

14 (*a*) S. G. Reis, M. Briganti, D. O. T. A. Martins, H. Akpinar, S. Calancea, G. P. Guedes, S. Soriano, M. Andruh, R. A. A. Cassaro, P. M. Lahti, F. Totti and M. G. F. Vaz, *Dalton Trans.*, 2016, **45**, 2936–2944; (*b*) H. Li, Z. Sun, J. Sun, L. Xi, J. Guo, G. Sun, J. Xie, Y. Ma and L. Li, *J. Mater. Chem. C*, 2018, **6**, 2060–2068; (*c*) K. Wang, J. Sun, L. Xi, J. Lu, P. Jing and L. Li, *Dalton Trans.*, 2019, **48**, 14383–14389.

15 (*a*) A. Rassat and H. U. Sieveking, *Angew. Chem., Int. Ed.*, 1972, **11**, 303–304; (*b*) J. Veciana, C. Rovira, M. I. Crespo, O. Armet, V. M. Domingo and F. Palacio, *J. Am. Chem. Soc.*, 1991, **113**, 2552–2561; (*c*) A. Rajca and S. Utamapanya, *J. Org. Chem.*, 1992, **57**, 1760–1767; (*d*) K. Inoue and H. Iwamura, *Angew. Chem., Int. Ed.*, 1995, **34**, 927–928; (*e*) D. A. Shultz, S. H. Bodnar and J. W. Kampf, *Chem. Commun.*, 2001, 93–94; (*f*) E. Fukuzaki and H. Nishide, *J. Am. Chem. Soc.*, 2006, **128**, 996–1001; (*g*) A. Rajca, M. Takahashi, M. Pink, G. Spagnol and S. Rajca, *J. Am. Chem. Soc.*, 2007, **129**, 10159–10170; (*h*) A. Rajca, K. Shiraishi and S. Rajca, *Chem. Commun.*, 2009, 4372–4374; (*i*) P. J. Boratyński, M. Pink, S. Rajca and A. Rajca, *Angew. Chem., Int. Ed.*, 2010, **49**, 5459–5462; (*j*) S. Suzuki, T. Furui, M. Kuratsu, M. Kozaki, D. Shiomi, K. Sato, T. Takui and K. Okada, *J. Am. Chem. Soc.*, 2010, **132**, 15908–15910; (*k*) W. Wang, L. Wang, S. Chen, W. Yang, Z. Zhang and X. Wang, *Sci. China: Chem.*, 2018, **61**, 300–305; (*l*) N. Gallagher, H. Zhang, T. Junghoefer, E. Giangrisostomi, R. Ovsyannikov, M. Pink, S. Rajca, M. B. Casu and A. Rajca, *J. Am. Chem. Soc.*, 2019, **141**, 4764–4774.

16 (*a*) D. A. Shultz, S. H. Bodnar, H. Lee, J. W. Kampf, C. D. Incarvito and A. L. Rheingold, *J. Am. Chem. Soc.*, 2002, **124**, 10054–10061; (*b*) M. L. Kirk and D. A. Shultz, *Coord. Chem. Rev.*, 2013, **257**, 218–233.

17 (*a*) T. Nokami, T. Matsuo, Y. Inatomi, N. Hojo, T. Tsukagoshi, H. Yoshizawa, A. Shimizu, H. Kuramoto, K. Komae, H. Tsuyama and J.-i. Yoshida, *J. Am. Chem. Soc.*, 2012, **134**, 19694–19700; (*b*) Y. Liang, Y. Jing, S. Gheytani, K.-Y. Lee, P. Liu, A. Facchetti and Y. Yao, *Nat. Mater.*, 2017, **16**, 841–848; (*c*) Y. Liang and Y. Yao, *Joule*, 2018, **2**, 1690–1706.

18 K. M. Kadish, W. E, R. Zhan, T. Khoury, L. J. Govenlock, J. K. Prashar, P. J. Sintic, K. Ohkubo, S. Fukuzumi and M. J. Crossley, *J. Am. Chem. Soc.*, 2007, **129**, 6576–6588.

19 J. Hicks, M. Juckel, A. Paparo, D. Dange and C. Jones, *Organometallics*, 2018, **37**, 4810–4813.

20 (*a*) S. P. Green, C. Jones and A. Stasch, *Science*, 2007, **318**, 1754–1757; (*b*) C. Jones, *Nat. Rev. Chem.*, 2017, **1**, 0059.

21 G. Tan, J. Li, L. Zhang, C. Chen, Y. Zhao, X. Wang, Y. Song, Y.-Q. Zhang and M. Driess, *Angew. Chem., Int. Ed.*, 2017, **56**, 12741–12745.

22 F. Spitzer, C. Graßl, G. Balázs, E. M. Zolnhofer, K. Meyer and M. Scheer, *Angew. Chem., Int. Ed.*, 2016, **55**, 4340–4344.

23 (*a*) G. Sheldrick, *Acta Crystallogr., Sect. C: Struct. Chem.*, 2015, **71**, 3–8; (*b*) CCDC 1998479–1998482 contain the supplementary crystallographic data for this paper.†

24 R. Lalrempuia, A. Stasch and C. Jones, *Chem. Sci.*, 2013, **4**, 4383–4388.

25 Z. Wang, V. Enkelmann, F. Negri and K. Müllen, *Angew. Chem., Int. Ed.*, 2004, **43**, 1972–1975.

26 S.-i. Kawano, M. Baumgarten, D. Chercka, V. Enkelmann and K. Müllen, *Chem. Commun.*, 2013, **49**, 5058–5060.

27 (*a*) R. E. Cowley, J. Elhaïk, N. A. Eckert, W. W. Brennessel, E. Bill and P. L. Holland, *J. Am. Chem. Soc.*, 2008, **130**, 6074–6075; (*b*) S. Meyer, C. M. Orben, S. Demeshko, S. Dechert and F. Meyer, *Organometallics*, 2011, **30**, 6692–6702.

28 P. Hao, Z. Yang, X. Ma, X. Wang, Z. Liu, H. W. Roesky, K. Sun, J. Li and M. Zhong, *Dalton Trans.*, 2012, **41**, 13520–13524.

29 (*a*) A. D. Becke, *J. Chem. Phys.*, 1993, **98**, 5648–5652; (*b*) M. J. Frisch, G. W. Trucks, H. B. Schlegel, G. E. Scuseria, M. A. Robb, J. R. Cheeseman, G. Scalmani, V. Barone, B. Mennucci, G. A. Petersson, H. Nakatsuji, M. Caricato, X. Li, H. P. Hratchian, A. F. Izmaylov, J. Bloino, G. Zheng, J. L. Sonnenberg, M. Hada, M. Ehara, K. Toyota, R. Fukuda, J. Hasegawa, M. Ishida, T. Nakajima, Y. Honda, O. Kitao, H. Nakai, T. Vreven, J. A. Montgomery Jr, J. E. Peralta, M. B. F. Ogliaro, J. J. Heyd, E. Brothers, K. N. Kudin, V. N. Staroverov, T. Kieth, R. Kobayashi, J. Normand, K. Raghavachari, A. Rendell, J. C. Burant, S. S. Iyengar, J. Tomasi, M. Cossi, N. Rega, N. J. Millam, M. Klene, J. E. Knox, J. B. Cross, V. Bakken, C. Adamo, J. Jaramillo, R. Gomperts, R. E. Stratmann, O. Yazyev, A. J. Austin, R. Cammi, C. Pomelli, J. W. Ochterski, R. L. Martin, K. Morokuma, V. G. Zakrzewski, G. A. Voth, P. Salvador, J. J. Dannenberg, S. Dapprich, A. D. Daniels, Ö. Farkas, J. B. Foresman, J. V. Ortiz, J. Cioslowski and D. J. Fox, in *Gaussian 09, Revision B.01*, Gaussian, Inc., Wallingford CT, 2010.

30 I.-R. Jeon, J. G. Park, D. J. Xiao and T. D. Harris, *J. Am. Chem. Soc.*, 2013, **135**, 16845–16848.

31 N. F. Chilton, R. P. Anderson, L. D. Turner, A. Soncini and K. S. Murray, *J. Comput. Chem.*, 2013, **34**, 1164–1175.